STRIP1, a core component of STRIPAK complexes, is essential for normal mesoderm migration in the mouse embryo

Hisham Bazzi[a,b,c,1], Ekaterina Soroka[b,c], Heather L. Alcorn[a], and Kathryn V. Anderson[a,1]

[a]Developmental Biology Program, Sloan Kettering Institute, New York, NY 10065; [b]Department of Dermatology and Venereology, University Hospital of Cologne, 50937 Cologne, Germany; and [c]Cologne Cluster of Excellence in Cellular Stress Responses in Aging-Associated Diseases (CECAD), University of Cologne, 50931 Cologne, Germany

Edited by Brigid L. M. Hogan, Duke University Medical Center, Durham, NC, and approved November 10, 2017 (received for review August 1, 2017)

Regulated mesoderm migration is necessary for the proper morphogenesis and organ formation during embryonic development. Cell migration and its dependence on the cytoskeleton and signaling machines have been studied extensively in cultured cells; in contrast, remarkably little is known about the mechanisms that regulate mesoderm cell migration in vivo. Here, we report the identification and characterization of a mouse mutation in striatin-interacting protein 1 (*Strip1*) that disrupts migration of the mesoderm after the gastrulation epithelial-to-mesenchymal transition (EMT). STRIP1 is a core component of the biochemically defined mammalian striatin-interacting phosphatases and kinase (STRIPAK) complexes that appear to act through regulation of protein phosphatase 2A (PP2A), but their functions in mammals in vivo have not been examined. *Strip1*-null mutants arrest development at midgestation with profound disruptions in the organization of the mesoderm and its derivatives, including a complete failure of the anterior extension of axial mesoderm. Analysis of cultured mesoderm explants and mouse embryonic fibroblasts from null mutants shows that the mesoderm migration defect is correlated with decreased cell spreading, abnormal focal adhesions, changes in the organization of the actin cytoskeleton, and decreased velocity of cell migration. The results show that STRIPAK complexes are essential for cell migration and tissue morphogenesis in vivo.

STRIP1 | STRIPAK | PP2A | mouse embryo | cell migration

Gastrulation and the subsequent movements of the mesoderm are essential for the generation of the body plan and patterning of mammalian embryos (1). Before gastrulation, the embryo proper is composed of a single pseudostratified epithelial layer, the epiblast. During gastrulation, beginning at embryonic day 6.25 (E6.25), cells of the posterior epiblast, the primitive streak, undergo an epithelial-to-mesenchymal transition (EMT). The ingressing cells immediately acquire mesenchymal properties and migrate away from the site of the streak to form two new germ layers, the mesoderm and the definitive endoderm (2–4). By E7.5, cells of the mesoderm layer have spread around the entire embryonic circumference. The early mesoderm cells give rise in sequence to distinct mesodermal populations: the extraembryonic mesoderm, cardiac and cranial mesoderm, lateral plate mesoderm, and paraxial mesoderm of the anterior somites (5). After E7.5, mesoderm cells that will contribute to the paraxial mesoderm continue to be added from progenitors in the streak to generate the more posterior somites. Epiblast cells at the anterior (distal) tip of the primitive streak at E7.5 undergo EMT, ingress, and then immediately undergo a mesenchymal-to-epithelial transition to give rise to the axial mesoderm, the node and notochordal plate (6–8).

The molecular processes and pathways that regulate the movements of the mesoderm cells are not well understood. It is well established that FGF signaling at the streak activates expression of the transcription factor SNAIL1, which in turn represses transcription of the E-cadherin gene, and down-regulation of E-cadherin is essential for mesoderm migration (9, 10). In the chick, directional migration of the nascent mesoderm appears to depend on chemorepulsion by FGF and Wnt3a ligands expressed at the primitive streak (11), but it is not clear whether the same signals operate in the mouse. The ability of mesoderm cells to migrate depends on a complete reorganization of the actin cytoskeleton, and motility depends on the WAVE complex and the small GTPase RAC1 (12, 13).

Experiments in cell culture recently implicated the striatin-interacting phosphatases and kinases (STRIPAK) complexes in the migration of mammalian cells (14). Striatins, core components of the complex, are calmodulin-binding WD-repeat proteins that were first identified based on their strong expression in the striatum of the mammalian brain (15). Striatin was shown to form a complex with the catalytic and regulator subunits of protein phosphatase 2A (PP2A) (16) and was then shown to be part of larger complexes that include the kinases STK24 (MST3), STK25, and STK26 (MST4), now called the STRIPAK complexes (17), that are conserved from fungi to humans (18).

There are more than 200 isoforms of the serine/threonine phosphatase PP2A, accounting for their diverse cellular functions (19). Each isoform includes a catalytic subunit, a scaffolding (A) subunit, and a regulatory (B) subunit (20). Striatins act as noncanonical B-type regulatory subunits for PP2A, controlling its localization and specificity. The STRIPAK complexes are

Significance

Striatin-interacting phosphatases and kinases (STRIPAK) complexes can regulate the cytoskeleton and cell migration in cell lines, but their roles in vivo in mammals are not known. Here, we show that mouse embryos that lack striatin-interacting protein 1 (STRIP1), a core component of STRIPAK complexes, arrest at midgestation with striking morphological defects. *Strip1* mutants lack a trunk, and both paraxial and axial mesoderm fail to elongate along the anterior–posterior body axis. Mesodermal cells from *Strip1* mutants have defects in actin organization, focal adhesions, and cell migration that can account for the failure of normal mesoderm migration. The findings demonstrate that STRIPAK is a critical regulator of mammalian cell migration and is likely to have important roles in tumor progression as well as development.

Author contributions: H.B. and K.V.A. designed research; H.B., E.S., H.L.A., and K.V.A. performed research; H.B., E.S., H.L.A., and K.V.A. analyzed data; and H.B. and K.V.A. wrote the paper.

The authors declare no conflict of interest.

This article is a PNAS Direct Submission.

[1]To whom correspondence may be addressed. Email: hisham.bazzi@uk-koeln.de or k-anderson@sloankettering.edu.

This article contains supporting information online at www.pnas.org/lookup/suppl/doi:10.1073/pnas.1713535114/-/DCSupplemental.

believed to regulate PP2A activity in response to the activity of the kinases within the complex; in addition, kinases within the STRIPAK can be substrates for the phosphatase activity of PP2A (18, 21, 22).

Mouse striatin-interacting protein 1 (*Strip1*), a core component of the STRIPAK, is a moderately large (837-aa) protein that lacks informative protein motifs. The in vivo functions of *Strip1* were described first in *Neurospora*, where *ham-2*, the *Strip1* homolog, and other components of the STRIPAK are required for hyphal fusion (23). The homologous budding yeast gene, *Far11*, was identified based on its requirement for normal recovery from pheromone arrest (24). *Neurospora* Ham-2 associates with a vesicular compartment (25) and the yeast FAR11 complex localizes to the endoplasmic reticulum (26, 27). The *Caenorhabditis elegans* homolog, *farl-11*, also localizes to the endoplasmic reticulum and is required for endoplasmic reticulum integrity (28).

We identified a mutation in mouse *Strip1* based on its profound disruption of the body plan. The absence of STRIP1 causes a dramatic shortening of the anterior–posterior axis, so that the head is connected directly to the tail and there is essentially no trunk. This embryonic phenotype is similar to the phenotype caused by the absence of RAC1 (12), suggesting a role for STRIP1 in RAC1-dependent cell motility. We show that the *Strip1* phenotype is caused by a failure of anterior–posterior elongation in both the axial and paraxial mesoderm due to the abnormal migration of these cell populations. Cell-based studies indicate that STRIP1 is essential for organization of the actin cytoskeleton and of focal adhesions, which are crucial for normal mesoderm migration. The dramatic phenotype of *Strip1* embryos highlights the important role of mesoderm cell behaviors in driving the elongation of the anterior–posterior body axis of the mouse embryo.

Results

Strip1 Is Essential for the Morphogenesis of the Early Mouse Embryo. In a genetic screen to isolate recessive mutations that disrupt mouse embryonic development at midgestation (29), we isolated a recessive mutant based on the striking abnormal morphology and early lethality of the mutant embryos. At E8.5, the anterior–posterior axis of the mutants was extremely short and appeared to consist of only a head connected to a swollen primitive streak, without an obvious trunk (Fig. 1*A*). One day earlier, at E7.5, the mutants were smaller than wild-type littermates, and about one-half of the mutants (44/84) showed a constriction at the embryonic/extraembryonic boundary; we therefore named this mutant "*cinchy*" (Fig. 1*B* and Fig. S1 *A*–*D*).

Embryos with the *cinchy* phenotype were isolated from several independently mutagenized males and the phenotype segregated with the backcross strain (29), suggesting that the *cinchy* mutation arose spontaneously in the nonmutagenized backcross (FVB/N) strain. Using classical genetic mapping, Sanger sequencing and next-generation sequencing (*Materials and Methods*), we identified a single change: a three-nucleotide (CTG) in-frame deletion in exon 16 of the gene *Strip1* (formerly known as *Fam40a* or *6330569M22Rik*), which encodes an 837-aa protein that is a core component of the STRIPAK complexes. This mutation would lead to the deletion of one leucine (L) in a highly conserved stretch of five leucines (amino acids 537–541) (Fig. S1*E*).

To assess the functional consequences of this in-frame deletion on the STRIP1 protein, we engineered constructs expressing either wild-type or mutant STRIP1 proteins fused to GFP and expressed them in HEK293T cells. Western blot analysis showed that the STRIP1^{cinchy}-GFP fusion protein was expressed at much lower levels (<15%) compared with the wild-type fusion protein (Fig. S1*F*), suggesting that the mutation greatly decreased the stability of the STRIP1 protein.

To confirm that the *Strip1* mutation caused the *cinchy* phenotype, we obtained mouse embryonic stem cells carrying a *Strip1* knockout-first allele from the International Knockout Mouse Consortium (IKMC) (30, 31) to generate both gene trap and null alleles of the gene. Transheterozygotes of *cinchy* with the gene trap (*Strip1*$^{cin/gt}$) allele showed the characteristic *cinchy* phenotype, as did the gene trap and null homozygotes (Fig. 1*A*). Western blot analysis using two different antibodies against endogenous STRIP1 showed that the protein could be readily detectable in wild-type but not null mutant E8.5 embryos or in mouse embryonic fibroblasts (MEFs) (*Materials and Methods*) derived from *Strip1*$^{gt/gt}$ embryos (Fig. 1 *C* and *D*), indicating that both *Strip1*^{gt} and *Strip1*$^{-}$ are null alleles of the gene. As the three alleles of *Strip1* (*Strip1*$^{cin/cin}$, *Strip1*$^{gt/gt}$, and *Strip1*$^{-/-}$) showed indistinguishable embryonic phenotypes, *cinchy* also appears to be a null or severe hypomorphic allele.

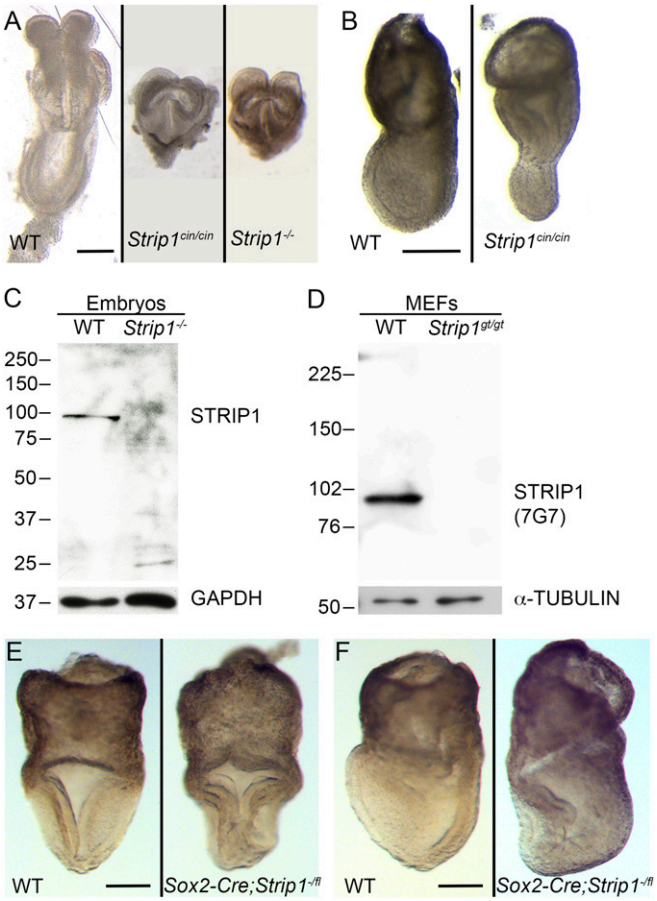

Fig. 1. *cinchy* is a mutant allele of *Strip1*, which is essential for embryonic morphogenesis. (*A*) Dorsal view of wild-type (WT), *cinchy* (*Strip1*$^{cin/cin}$), and *Strip1*$^{-/-}$ embryos at E8.5. Note the defect in body elongation in *cinchy* and *Strip1*$^{-/-}$ embryos, which show almost identical phenotypes, compared with WT. Anterior is up. (*B*) Side view of a WT and a *Strip1*$^{cin/cin}$ mutant at E7.5 with a cinch in the mutant. Posterior is to the *Right*. (*C* and *D*) Western blot analysis using anti-STRIP1 antibodies on WT and *Strip1*$^{-/-}$ embryos at E8.5 as well as MEFs lysates derived from WT and *Strip1*$^{gt/gt}$ embryos (STRIP1 antibody clone 7G7). STRIP1 is not detectable in the *Strip1* mutant embryos or MEFs compared with WT. (*E* and *F*) Anterior (*E*) and side (*F*) views of WT and *epiblast-deleted* (*Sox2-Cre*) *Strip1* mutant embryos at E7.5. Note the absence of the cinch but abnormal head folds in the mutant. $n \geq 4$ embryos per genotype. (Scale bars: 300 μm.)

STRIP1 Acts in Epiblast-Derived Cells and Is Required for Paraxial Mesoderm Morphogenesis. At E7.5, *Strip1* mRNA was expressed in all of the germ layers of wild-type embryos but was expressed at highest levels in in the mesoderm layer (Fig. S2 *A* and *B*), suggesting that it could act in the mesoderm cells during the time that they are migrating. At later stages, *Strip1* mRNA and protein

were more broadly expressed and present in both the mesoderm and neural ectoderm (Fig. S2 *C* and *D*). At the subcellular level, a STRIP1-GFP fusion protein transiently transfected into mIMCD3 epithelial cells or MEFs was enriched in the perinuclear area; it was also enriched in cellular protrusions in MEFs (Fig. S2 *E* and *F*, arrowheads).

To test whether STRIP1 was required in embryonic or extraembryonic lineages, we generated a *Strip1* conditional allele from the knockout-first allele (*flox*, *fl*; *Materials and Methods*) and crossed it to the *Sox2-Cre* transgenic line, which expresses the Cre recombinase only in the epiblast and its derivatives (the "embryo proper") but not in extraembryonic lineages (32). The E7.5 *Strip1 epiblast-deleted* embryos lacked the constriction at the embryonic/extraembryonic border (Fig. 1 *E* and *F*), but at E8.5 showed the same profound defects in body elongation seen in the embryos that lacked the gene in all lineages (Fig. 2).

Despite the clearly abnormal morphology of the *Strip1* mutant embryos, many aspects of tissue organization appeared normal in the mutants. Proliferation, as judged by the mitotic index, was not significantly different in either whole E7.5 mutant embryos or individual germ layers, relative to wild type [wild type: 7.6 ± 1.2% (total) and 7 ± 1% (mesoderm); mutant: 6.7 ± 0.4% (total) and 6 ± 1% (mesoderm); $P = 0.37$ (total) and 0.38 (mesoderm)]. The organization and polarity of the E8.5 neural and epiblast epithelium appeared normal: ZO1, a tight junction protein, was localized apically; GM130, a *cis*-Golgi marker, and F-Actin were apically enriched in both wild type and mutant; RAB11 was enriched in apical vesicles in both wild type and mutant (Fig. S3).

In contrast, analysis of the expression of cell type-specific markers revealed profound defects in the morphogenesis of mesodermal tissues in the mutants. Nascent mesoderm, marked by the expression of *Tbx6*, was specified in E8.5 *Strip1* mutants, but the *Tbx6*-positive (+) cells failed to move away from the streak and instead accumulated in a midline ridge that overlapped with the domain of *Brachyury* (*T*) expression (Fig. 2 *A* and *B*). Paraxial mesoderm gives rise to the segmented somites of the trunk. It appeared that fewer paraxial mesoderm cells, marked by expression of *Meox1*, were specified in the mutant (Fig. 2*C*). Most strikingly, the *Meox1*+ cells failed to extend in the anterior–posterior axis and no segmented somites were detected in either the *Strip1*$^{-/-}$ or *Strip1 epiblast-deleted* embryos (Fig. 2*C*). The mesoderm cells of the heart primordium, marked by *Nkx2.5*, were specified and formed a cardiac crescent in *Strip1* mutant embryos, but they failed to converge to the midline to generate the single heart tube (Fig. 2*D*).

STRIP1 Is Required for the Organization of the Axial Mesoderm. Analysis of cell type-specific markers by in situ hybridization showed that the axial mesoderm was profoundly disrupted in the mutants. *T* is expressed in both the primitive streak and in the thin line of axial mesoderm of E8.5 wild-type embryos. In contrast, *T* was expressed in a short broad strip in E8.5 *Strip1* mutants that appeared to correspond to the streak and a very short midline (Fig. 2*B*). Sonic hedgehog (*Shh*), which is expressed in the midline of wild-type embryos, was expressed in a short patch on the midline (axial mesoderm and floor plate) of the *Strip1* mutants (Fig. 3*A*, arrowheads). *Foxa2* is expressed in the axial mesoderm and the endoderm in wild type (Fig. 3*B*). Consistent with the *T* and *Shh* expression patterns, the axial mesoderm domain of *Foxa2* was reduced to a small spot in the *Strip1* mutants (Fig. 3*B*, arrowheads). Thus, the axial mesoderm was reduced and failed to extend anteriorly in the mutants.

To assess the organization in the axial mesoderm at cellular resolution, we examined the distribution of F-Actin and expression of T protein at E7.75 by immunostaining (Fig. 3*C*). The node is a transient cup-shaped structure that, together with the notochordal plate, occupies the ventral midline of the embryo. The mesendodermal cells forming the node and the notochordal plate are highly polarized and have constricted apical surfaces, so these cells can be clearly marked by enriched apical F-Actin and nuclear T expression. Based on T expression, the mutant node was small and irregular in shape (Fig. 3*C*) and the notochordal plate was short and failed to extend in *Strip1* mutants compared with wild type (Fig. 3*C*).

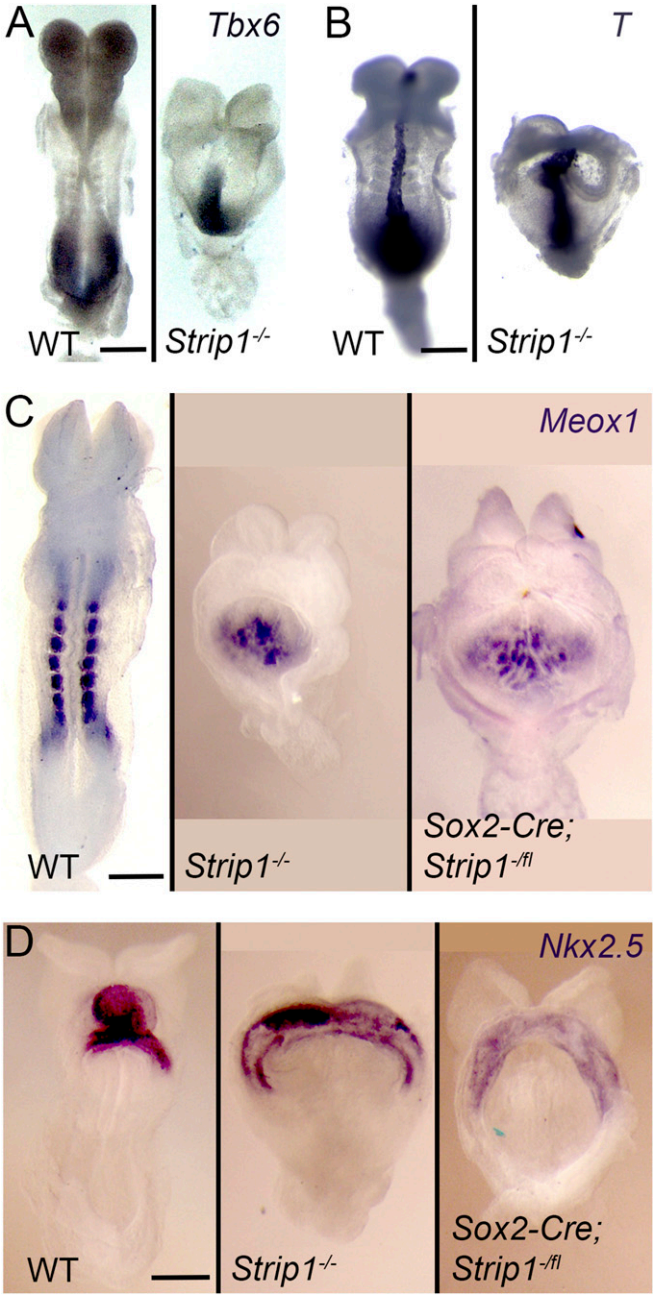

Fig. 2. STRIP1 acts in cells derived from the epiblast to organize the paraxial mesoderm. (*A*) Dorsal view of WT and *Strip1* mutant embryos at E8.5 showing the accumulation of *Tbx6*+ cells, using in situ hybridization, at the bulging primitive streak in the mutant. (*B*) Ventral view of WT and *Strip1* mutant embryos at E8.5 showing in situ hybridization signals using *T* (streak and axial mesoderm). (*C* and *D*) Ventral view of WT, *Strip1*$^{-/-}$, and *epiblast-deleted* (*Sox2-Cre*) *Strip1* mutant embryos at E8.5 showing in situ hybridization signals using *Meox1* (somites) and *Nkx2.5* (heart) markers. The *epiblast-deleted Strip1* mutant is similar to the null mutant and both have a deficit and/or abnormal morphogenesis of the paraxial and cardiac mesoderm. $n \geq 3$ embryos per genotype. Anterior is up in all panels. (Scale bars: 300 μm.)

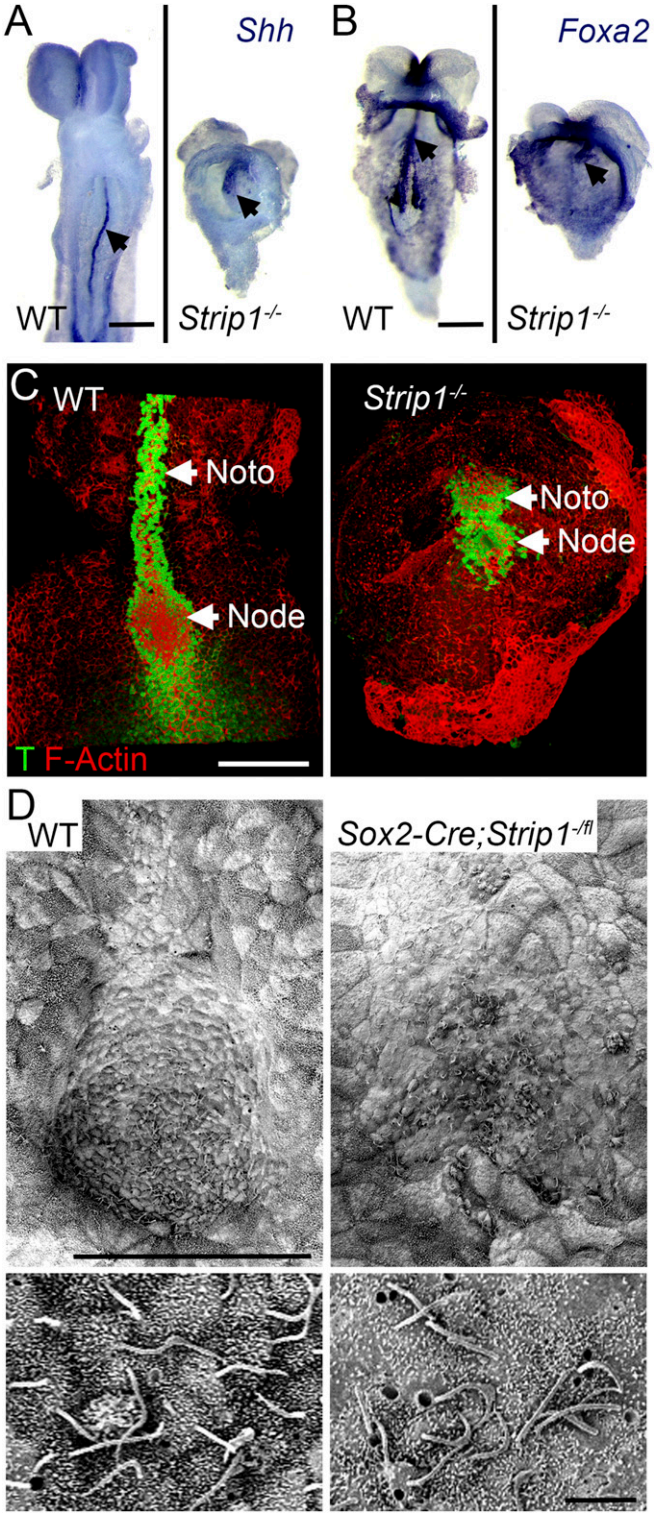

Fig. 3. Morphogenesis of the node and notochordal plate is defective in *Strip1* mutants. (*A* and *B*) Ventral view of WT and *Strip1* mutant embryos at E8.5 showing in situ hybridization signals using *Shh* (midline) and *Foxa2* (midline and endoderm) probes. The mutants have clear defects in body elongation and axial mesoderm formation. $n \geq 5$ embryos per genotype. (*C*) Ventral view of 3D images of WT and *Strip1* mutant embryos at E7.75 stained with a T antibody (green; axial mesoderm and streak) and F-Actin (phalloidin; red). The node and notochordal plate (Noto) regions in the mutant are wide and fail to extend anteriorly. $n \geq 5$ embryos per genotype. (*D*) Scanning electron microscopy (SEM) images of the node in WT and *Strip1* mutant embryos at E7.5. The mutant node, with ciliated cells (magnification of the center of the node, *Bottom*), has an irregular flat shape compared with the cup-shaped WT node. $n \geq 2$ embryos per genotype. Anterior is up in all panels. (Scale bars: *A–D*, 300 μm; *D*, *Bottom*, 3 μm.)

Each cell of the cup-shaped node extends a long single cilium that can be visualized by scanning electron microscopy (SEM) at E7.75 (Fig. 3*D*). Scanning electron micrographs of the node showed that the cilia-bearing node cells formed an irregular and flat plate in the *Strip1* mutant, in contrast to the pit structure typical of wild type (Fig. 3*D*).

The *Strip1* Phenotype Is Caused by Abnormal Migration of the Mesoderm. A shortened anterior–posterior axis is frequently associated with a deficit in mesoderm and has been seen both in mutants that disrupt formation of mesoderm during the gastrulation EMT and in mutants that interfere with migration of the mesoderm. In both classes of mutants, extra cells accumulate in the region of the primitive streak: cells accumulate in the epiblast layer in mutations that disrupt the EMT, and cells accumulate in the mesoderm layer below the streak in mutants with defective mesoderm migration (4, 8, 12, 13, 33).

To determine the origin of the mesoderm defects in *Strip1* mutants, we examined the primitive streak region of E7.5 and E8.5 embryos. By staining for SOX2, SNAIL1, and LAMININ1 (LAM) in E7.5 embryo sections, we found that the primitive streak formed where the basement membrane was broken, as marked by the position of LAM expression (Fig. 4*A*, vertical bar), and the mesodermal cells had spread around the embryonic circumference (Fig. 4*A*, arrowheads). SOX2 expression was limited to the epiblast, and SNAIL1 was correctly expressed in the nascent mesoderm, indicating that the SOX/SNAIL switch took place normally (34) (Fig. 4*A*). However, some SNAIL1+ nascent mutant mesodermal cells accumulated near the E7.5 streak (Fig. 4*A*, arrows). Staining for E-cadherin (E-CAD) and N-cadherin (N-CAD), to mark the epiblast epithelium and mesoderm, respectively, showed the greater thickness of the mutant mesodermal wings at E7.0 (Fig. 4*B*, arrowheads) and the accumulation of mesoderm cells near the mutant streak at E7.5 (Fig. 4*C*, arrows). The endoderm layer in E7.5 *Strip1* mutant embryos expressed endodermal markers (SOX17 and FOXA2; Fig. S4*A*) and showed normal apical/basal polarity (Fig. S4*B*), but formed a cuboidal rather than the squamous endoderm layer (Fig. 4 *A–C*). As the endoderm layer in E7.5 embryos forms by intercalation of definitive endoderm cells originating from the mesoderm layer into the visceral endodermal layer (35), the intercalation process may be delayed or abnormal in *Strip1* mutants.

By E8.5, the accumulation of mesoderm cells near the streak in *Strip1* mutant embryos was much more prominent (Fig. 4*D*). SNAIL1+ cells in E8.5 wild-type embryos moved efficiently away from primitive streak site, whereas SNAIL1+ cells in E8.5 *Strip1* embryos accumulated adjacent to the streak, causing the epiblast to bulge into the amniotic cavity (Fig. 4*D*). Altogether, the data indicate that STRIP1 is not required for the EMT but is required for normal mesoderm cell migration at E7.0 and later stages.

Actin Organization, Focal Adhesions, and Migration Are Disrupted in *Strip1* Mesodermal and Mesenchymal Cells. To confirm that the disruption of the organization of the embryonic mesoderm was due to autonomous changes in mesoderm cell behavior, we cultured explants of the mesodermal germ layer dissected from E7.5 *Strip1* and wild-type embryos (*Materials and Methods*) (Fig. 5*A*). Wild-type cells that had migrated out of mesodermal explants were well-spread and showed typical lamellipodia and filopodia morphology, as well as F-Actin in stress fibers at 48 h. Wild-type cells had many well-defined focal adhesion contacts, marked by VINCULIN (VIN). In contrast, mutant mesoderm cells appeared much more compact, with enriched cortical F-Actin

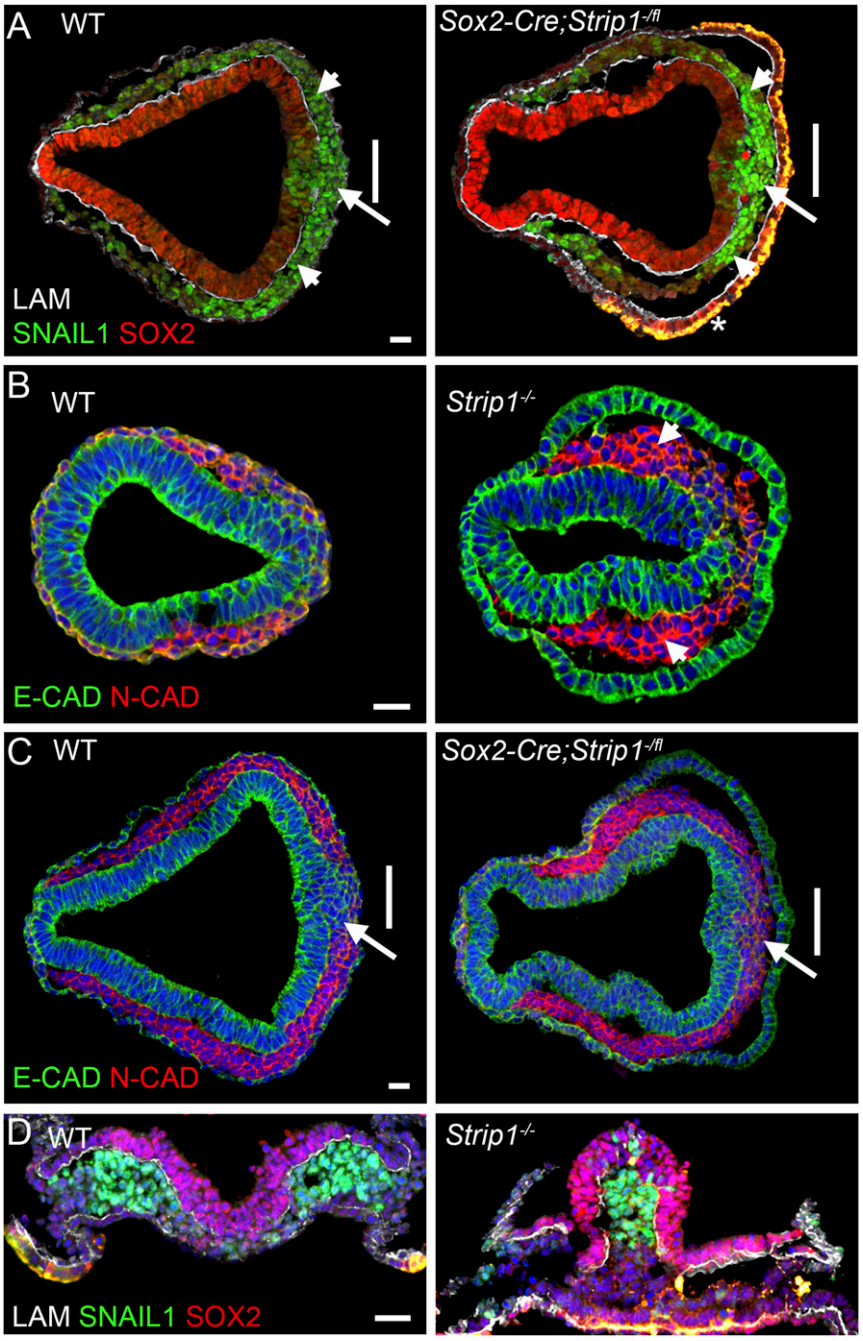

Fig. 4. Defects in mesoderm migration in *Strip1* mutant embryos. (*A–C*) Cross-sections of E7.0–E7.5 WT and *Strip1* mutant embryos. The region of the streak is marked with a vertical line, the nascent mesoderm adjacent to the streak is marked by an arrow, and the mesodermal wings are indicated by arrowheads. The asterisk (*) indicates nonspecific staining in the visceral endoderm cells. Note the variable thickness of the mesoderm layer and the cuboidal shape of endodermal cells in the mutants (*A–C*). The extent of the interruption of the basement membrane (LAM), which marks the position of the primitive streak, appears the same in the *Strip1* mutants as in WT. (*A*) SNAIL1+ cells accumulate near the streak (arrows). (*B* and *C*) The E-CAD to N-CAD switch is normal in the mutant embryos, but the N-CAD+ mesoderm wings are thicker (*B*) and accumulate near the streak (*C*). (*D*) Cross-sections of E8.5 WT and *Strip1* mutant embryos show a greater accumulation of mesoderm cells adjacent to the primitive streak than at earlier stages. The epiblast is marked by expression of SOX2 (red), SNAIL1 (green) marks the nascent mesoderm, and the position of the break in LAM (white) marks the position of the primitive streak. The SOX2 to SNAIL1 switch is normal in *Strip1* mutant embryos. $n \geq 6$ embryos per genotype. Posterior is to the *Right* in *A–C*. The epiblast is at the top, and endoderm is down in *D*. (Scale bars: 30 μm.)

and a smaller surface area, and the focal adhesions appeared to be fused and fewer in number (Fig. 5*A*).

For more quantitative analyses, we used the MEFs derived from *Strip1* mutant embryos. Mutant MEFs were less spread than controls, with an area only ~40% (~1,800 versus ~4,600 μm^2, $P < 0.0001$) that of control cells (Fig. 5 *B* and *C*). This contracted phenotype of *Strip1* mutant cells was similar to the phenotype seen after *Strip1* knockdown in several cell lines (14, 36) and was consistent with the cell shape change in the endoderm (Fig. 4 *A–C*). Cortical F-Actin was enriched in the *Strip1* mutant cells compared with control MEFs, perhaps contributing to the smaller cell area ($P = 0.0003$; Fig. 5*D*), and the mutant MEFs were more circular

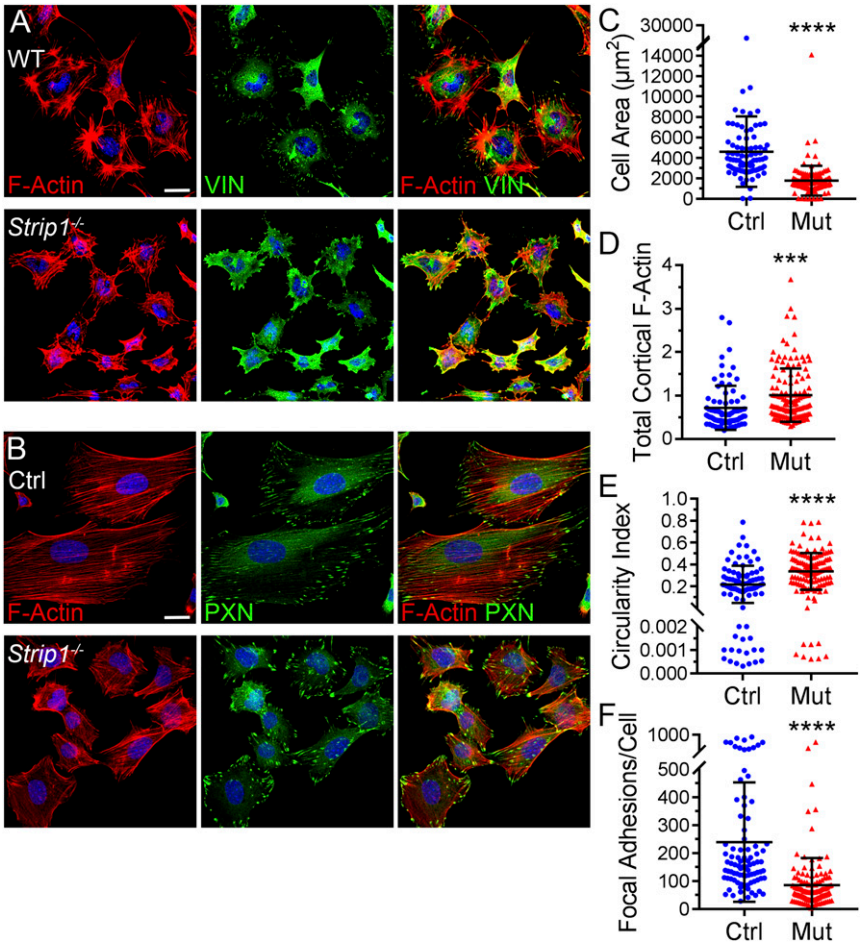

Fig. 5. Cell spreading, actin organization, and focal adhesion defects in *Strip1* mutant cells. (*A* and *B*) Immunofluorescent staining of mesodermal explants (*A*) and MEFs (*B*) from control (Ctrl) and *Strip1* mutant (Mut) embryos using F-Actin (red, phalloidin) and VINCULIN (*A*, VIN in green) or PAXILLIN (*B*, PXN in green). (*C*) Quantification of the cell area (in square micrometers) based on F-Actin staining. ****$P < 0.0001$; Ctrl, 4,610 ± 3,446 μm^2, $n = 84$; Mut, 1,773 ± 1,456 μm^2, $n = 123$. (*D*) Quantification of cortical F-Actin fluorescence intensity, 4 μm from the cell edge normalized to that of the cytoplasm. ***$P = 0.0003$; Ctrl, 0.72 ± 0.51, $n = 83$; Mut, 1.01 ± 0.61, $n = 137$. The total cellular F-Actin intensity (arbitrary units) per square micrometer was not significantly different. $P = 0.22$; Ctrl, 3,251 ± 1,130; Mut, 3,081 ± 923. (*E*) Quantification of the circularity index. ****$P < 0.0001$; Ctrl, 0.22 ± 0.17, $n = 84$; Mut, 0.34 ± 0.17, $n = 127$. (*F*) Quantification of the number of focal adhesions per cell based on PXN staining. ****$P < 0.0001$; Ctrl, 239 ± 214, $n = 89$; Mut, 85 ± 97, $n = 135$. All quantifications on MEFs were performed on cells from four independent Ctrl or *Strip1* Mut MEF lines. The data are presented as the mean ± SD. (Scale bars: 30 μm.)

than control cells ($P < 0.0001$; Fig. 5*E*). The mutant MEFs had about one-third as many focal adhesion contacts per cell as present in control MEFs (an average of 85 versus 239 per cell; $P < 0.0001$; Fig. 5*F*), as assayed by PAXILLIN (PXN) foci, and the average area of each focal contact in mutants was more than double that of control MEFs (4.7 ± 3.6 versus 2.0 ± 1.0 μm^2; $P < 0.0001$) suggesting that focal adhesions may be clustered.

We performed scratch healing assays on confluent MEF cultures and recorded live videos of the cells migrating and closing the gap (Fig. 6*A* and Movies S1 and S2). The *Strip1* mutant MEFs took ∼6–10 h (494 min) to close the scratch, ∼1.6 times longer than control MEFs, which closed the scratch in 4–6 h (307 min; $P = 0.03$) (Fig. 6*B*). The delay in closing the scratch was due to a slower velocity of migration: the *Strip1* mutant MEFs migrated 30% more slowly than control cells on average (0.40 versus 0.58 μm/min, $P < 0.0001$; Fig. 6*C*). A subset of *Strip1* mutant MEF cells appeared to pause during migration, showing no movement in higher fraction of the frames than in controls (5% versus 1%, $P < 0.0001$; Fig. 6*D*). Even without including the data from paused cells, the velocity of migrating *Strip1* mutant MEFs was significantly less than that of the controls (0.48 ± 0.24 versus 0.69 ± 0.41 μm/min; $P < 0.0001$). The migrating *Strip1* mutant MEFs had ∼30% more filopodia-like and F-Actin–based protrusions at the leading edge compared with controls (12.2 ± 4.7 versus 9.5 ± 3.3 per cell; $P < 0.0001$; $n = 130$ and 97 for mutant and control, respectively).

Discussion

The data show that STRIP1 is required for normal migration of the mesoderm in the mouse embryo. In the absence of STRIP1, the full range of mesodermal cell types is specified, but both paraxial and axial mesoderm fail to elongate in the anterior–posterior axis. Because STRIP1 mutant mesodermal cells show profound defects in cell shape, actin organization, focal adhesions, and cell movement, we infer that STRIP1 acts in mesoderm cells to promote cell migration and that normal mesoderm migration is essential for the organization of the body axis. The defect in the anterior–posterior extension of the mesoderm is especially striking and suggests that STRIP1 has a central role in the process of convergent extension of the mesoderm (37, 38).

The failure of axis elongation in *Strip1* mutants is likely to be due to the loss of the integrity of the STRIPAK complex, as the only known role of STRIP1 is as a core component of the complex (17). Mice carrying a targeted null mutation in mouse *Strip2* (also

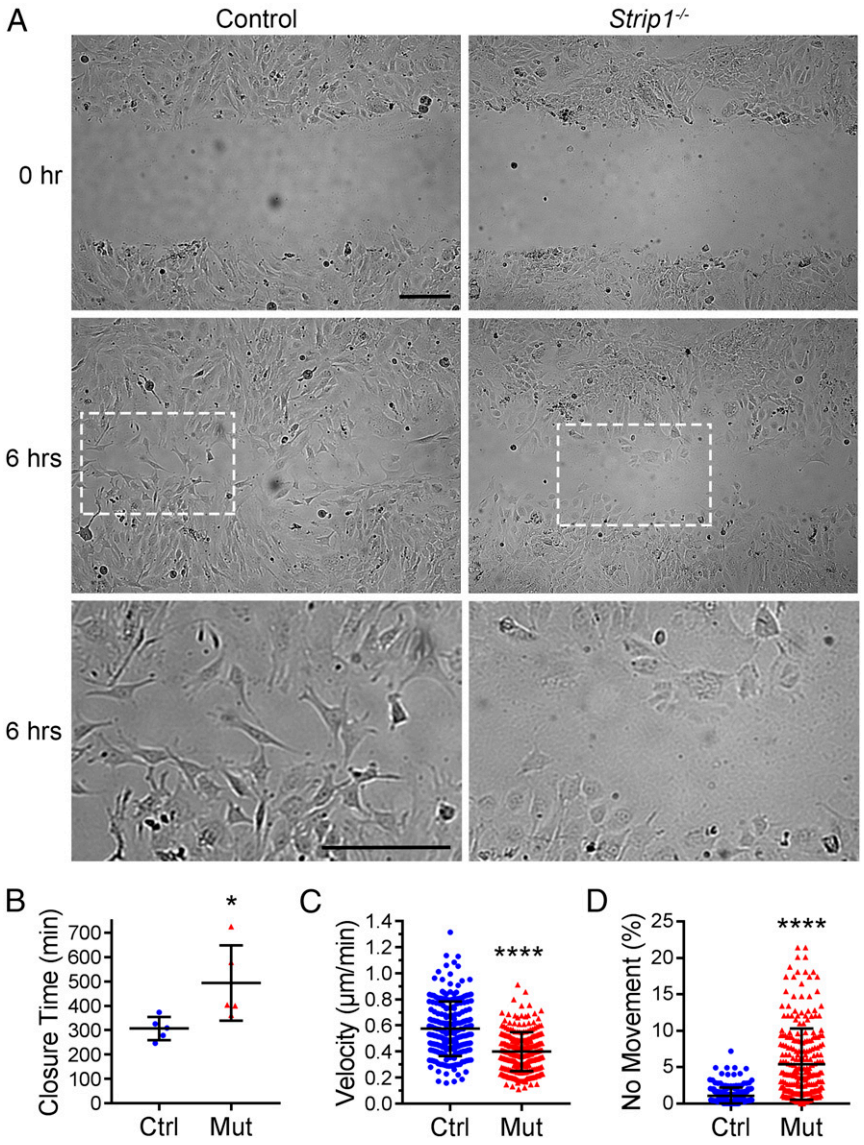

Fig. 6. *Strip1* mutant MEFs migrate slowly in scratch assays. *Strip1* mutant cells take longer to close the scratch, move at slower velocities, and take more pauses while migrating. (*A*) Snapshots from Movies S1 and S2 showing the control (Ctrl) and *Strip1* mutant (Mut) MEFs at the beginning (0 h) and at 6 h after performing the scratch. Dotted rectangles at 6 h indicate the zoomed images (*Bottom* row). Note the smaller area and protrusions of the mutant cells. (*B*) Quantification of the time to close the scratch (in minutes) from Ctrl and Mut MEF lines. Four independent MEF lines of each genotype were used. $^{*}P = 0.03$; Ctrl, 307 ± 48 min; Mut, 494 ± 155 min. (*C*) Quantification of the velocity of the cells (micrometer per minute) from three independent Ctrl or Mut MEF lines. $^{****}P < 0.0001$; Ctrl, 0.58 ± 0.21 μm/min, $n = 219$; Mut, 0.40 ± 0.15 μm/min, $n = 255$. (*D*) Quantification of the fraction of cases (in percentage) in which the cell showed no movement or displacement between frames in the scratch assay. $^{****}P < 0.0001$; Ctrl, 1 ± 1%; Mut, 5 ± 5%. The data are presented as the mean ± SD. (Scale bar: 30 μm.)

known as *Fam40b*), the paralog of *Strip1*, are viable and fertile, with physiological heart defects in older animals (39, 40). Thus, STRIP2 has only a subtle function in vivo, despite the strong phenotypes reported in cell-based knockdowns (14), whereas STRIP1 has an essential, nonredundant function in the embryo. In contrast, other components of the STRIPAK complexes are likely to have overlapping roles; there are, for example, three mouse *Striatin* genes and mutations in *Stm3* lead to cardiovascular defects in late in gestation (41). The dramatic phenotype caused by the absence of STRIP1 in the early embryo suggests that STRIPAK is likely to be a general regulator of cell migration that is used in both development and tumor progression, as suggested by misexpression of the components of the STRIPAK in tumors (14).

PP2A is likely to be a major effector of the STRIPAK complexes, and mouse mutations have implicated PP2A in mesoderm cell migration. Mouse embryos homozygous for a null allele of the gene encoding one of the two PP2A catalytic subunits, *Ppp2ca*, survive until after implantation but lack mesoderm (42, 43). Recently, it was reported that a null mutation in the Aα scaffolding subunit of the holoenzyme, encoded by *Ppp2r1a*, also causes embryonic lethality at the time of gastrulation (44) and that the classical mouse mutation *tw18* (45) is caused by a deletion of the *Ppp2r1a* gene. As originally described, *tw18* homozygotes survive past gastrulation, with an enlarged primitive streak and partial or complete duplication of the neural tube. Another mutation in the same complementation group, t^9 (46), also causes lethality at around E9 (47). Ultrastructural analysis of the mesoderm in early t^9 homozygotes defined specific defects in the organization of the mesoderm and the structure of projections on mesodermal cells (48), supporting a key role for PP2A in mesoderm migration.

Although not a core component of the STRIPAK complex, the kinase MAP4K4 can associate with STRIPAK complexes

through binding to STRN4 (49). The morphology of embryos that lack *Map4k4* is strikingly similar to that of *Strip1* mutants (50). Like *Strip1* mutants, *Map4k4* (*Nik*) mutant embryos arrest before embryonic turning at ∼E9.0, lack somites, and accumulate *T*+ and *Tbx6*+ cells in a bulged primitive streak region, suggesting that the two proteins may act in a common process. Loss of MAP4K4 from endothelial cells or mouse skin epithelial cells impairs cellular migration by reducing the speed of focal adhesion disassembly (51, 52).

Knockdown experiments suggested that STRIP1 determines the mode of cell migration in human epithelial cell lines through the regulation of the contractility of the actomyosin cortex and its connection to the plasma membrane (14). Knockdown or overexpression of *Strip1* in PC3 cells, a prostate cancer epithelial cell line, led to cell spreading defects, indicating that the level of STRIP1 is important for cytoskeletal organization and cell spreading (36), consistent with our findings in fibroblasts.

The data show that STRIP1 is required for mesenchymal cell migration and is enriched in cellular protrusions in mesenchymal migrating cells. As a major proposed role for the STRIPAK complexes is to compartmentalize the activity of the PP2A phosphatase and balance its activity with the associated kinases. we suggest that the STRIPAK complex in embryonic mesenchymal cells regulates the activity of PP2A to coordinate actin organization and focal adhesions during the directed cell migration that is required for elongation of the anterior–posterior body axis during embryogenesis.

Materials and Methods

Animals, Genotyping, and Mapping of the *cinchy* Mutation. The *Strip1* knockout-first ES cell line (EPD0316_1_G03) was obtained from the IKMC (*Strip1*$^{tm1a(KOMP)Wtsi}$) (www.mousephenotype.org/data/alleles/MGI:2443884/tm1a(KOMP)Wtsi). The null allele was generated by crossing *Strip1*$^{tm1a(KOMP)Wtsi}$ mice to *CAGG-Cre* mice (53). *Actin-FLP* transgenic mice [B6.Cg-Tg(ACTFLPe)9205Dym/J; Jax stock #005703] (54) were used to excise the gene trap and obtain the *Strip1*$^{+/fl}$ (fl, floxed allele) conditional allele. *Sox2-Cre* transgenic mice were used to delete *Strip1* from all embryonic tissues excluding the extraembryonic lineages (32). It is important to note that another *Strip1* knockout-first cell line EPD0316_1_A02 had a mixture of improperly targeted and correctly targeted ESC clones, based on Southern blotting, and was not used in this study. Phenotypes were analyzed in the FVB/NJ background. Genotyping was carried out using standard PCR protocols. Animals were housed and bred under standard conditions in accordance with Institutional Animal Care and Use Committee (IACUC) guidelines. The Memorial Sloan Kettering Cancer Center (MSKCC) IACUC and Landesamt für Natur, Umwelt, und Verbraucherschutz Nordrhein-Westfalen (LANUV) approved the experiments.

To genetically map the *cinchy* mutation, which segregated with the FVB/N DNA, the mice carrying the *cinchy* mutation were crossed to C57BL/10J. SNP mapping narrowed down the interval containing the mutation to ∼0.3 Mb in distal chromosome 3 (rs49331364: 107.384293 Mb to rs29591692: 107.748461 Mb), which harbors nine protein-coding genes. Using Sanger sequencing as well as SOLiD next-generation sequencing (Thermo Fisher Scientific) of the entire genomic interval identified a three-nucleotide (CTG) in-frame deletion in exon 16 of the gene *Strip1* leading to the deletion of one leucine (L) in a highly conserved stretch of five leucines (amino acids 537–541).

Embryo Explant and Cell Culture. For embryo mesodermal explant cultures, embryos were dissected at E7.5 and incubated in a pancreatin/trypsin mixture on ice for 20 min, and the germ layers were separated and cultured, as described elsewhere (10, 13). The explants were cultured on fibronectin-coated chamber slides (LabTek) at 37 °C with DMEM supplemented with 10% FBS and 1% penicillin–streptomycin (Thermo Fisher Scientific).

MEFs were prepared from E8.5 embryos by removing the heart and triturating before seeding onto gelatin-coated and cell culture-treated 12-well plates. MEFs were cultured in the same media as above. Immortalized MEF lines were derived from double-mutant embryos that lacked both *Strip1* and *p53* (*Trp53*^{tm1Tyj} null allele; The Jackson Laboratory; stock no. 002080) with *p53* mutant controls, and were used at passages 6–12.

Constructs, Immunofluorescence, Imaging, and Image Analyses. To generate the wild-type and mutant STRIP1-GFP fusion proteins, the corresponding *Strip1* cDNA was PCR amplified from wild-type or mutant cDNA and subcloned into a pEGFP-N1 vector using SacI (forward primer: TTAGAGCTCGTGTGGAGCAGCCAAGATGGAG) and XmaI (reverse primer: TTACCCGGGTTCTGCAGCAGCTCTTCCCAGGAA) restriction sites. Transient transfections of the plasmids were carried out using Lipofectamine 2000 or 3000 (Thermo Fisher Scientific) according to the manufacturer's recommendations. Cryosections of embryos were prepared using standard conditions (55). Immunofluorescence staining on whole embryos, embryo sections, and cells was performed using 4% paraformaldehyde fixation, 1× PBS, and 0.1% Triton X-100 wash buffer, appropriate-sera (10%) blocking, and the corresponding primary antibodies overnight at 4 °C. Images were obtained using Leica SP5 or SP8 confocal microscopes (Leica Microsystems) unless otherwise stated. Confocal images were analyzed using the Volocity software package (Improvision).

The mitotic index was calculated based on the ratio of phosphohistone-H3 (mitotic cells) and DAPI (total cells) stainings using the Cell Counter plug-in in ImageJ (NIH). n = 3,000–4,000 cells (total) and 1,000–1,400 cells (mesoderm) from two to three whole embryos of each genotype.

The scratch assay was performed on confluent cultures of the four independent MEF lines of each genotype grown on gelatin-coated 35-mm cell culture dishes (Falcon). The scratches were performed using a sterile tip, and the videos were captured using 4× objective fitted on a JuLi Br Live Cell Analyzer (Peqlab) at 10-min intervals for 12 h. The experiment was performed four times on different independent MEF lines. The cell velocity (in micrometers per minute) was calculated from three independent lines of each genotype in three independent experiments using the position of the nucleus with the Manual Tracking plug-in in ImageJ and the Chemotaxis and Migration Tool, version 2.0 (ibidi).

For the measurements in Fig. 5 of cell area, F-Actin, and focal adhesions, the four independent lines of MEFs from each genotype were cultured on gelatin-coated coverslips, and then stained with paxillin and rhodamine-conjugated phalloidin and imaged under a 63×, 1.4 N.A. oil objective fitted onto a Leica DM2000 wide-field microscope using a Leica DFC 450C camera. The cell area and circularity measurements were performed using ImageJ. The total cortical actin (4 μm from the cell edge) normalized to cytosolic actin was quantified using the QuimP (version 17.06.02) plug-in in ImageJ. The number and area of focal adhesions were based on paxillin staining and quantified as described (56).

For the analyses of cellular protrusions, the four independent lines of MEFs from each genotype were cultured on ibidiTreat eight-well μ-slides fitted with two-well silicone culture inserts, the inserts were removed 24 h later to create a standardized gap, and then the cells were left to migrate into the gap for ∼2 h to be fixed and stained with rhodamine-conjugated phalloidin and GM130 (a Golgi marker to indicate the leading edge of migration). The images were acquired under a 20×, 0.72 N.A. objective with 1.7× digital zoom on a Leica SP8 and analyzed manually for protrusions at the leading edge using ImageJ. A lamellipodium was counted as one cellular protrusion, and most of the protrusions on the mutant MEFs were small filopodia.

LacZ Staining and in Situ Hybridization. β-Galactosidase activity was detected and whole-mount in situ hybridization was performed on embryos following standard methods (55). The *Strip1* in situ probe was amplified with the following primers: forward, AGAGGGCTGGAAAAGACCAT; reverse, AAAACCCCACCATGACACC. The embryos were photographed using an HRC Axiocam (Zeiss) fitted onto a Leica stereomicroscope (Leica).

Western Blot Analysis. Embryos were dissected in cold 1× PBS with 0.1% Tween 20 and frozen at −80 °C to be lysed later in Laemmli buffer (Bio-Rad). Western blots were performed according to standard protocols. The luminescent detection reaction was performed using ECL Plus or Prime reagent (Amersham) according to the manufacturer's recommendations.

Antibodies. The following primary antibodies were used in this study: mouse anti-Snail1 (1/200; a kind gift from Antonio García de Herreros, Institut Hospital del Mar d'Investigacions Mèdiques, Barcelona, Spain); mouse anti-STRIP1 (clone 7G7; 1/1,000; Origene); rabbit anti-STRIP1 (1/5,000; Bethyl Laboratories); mouse anti-SOX2 (E-4; 1/2,000; Santa Cruz Biotechnology); rabbit anti-pericentrin (1/3,000; Biolegend); rabbit anti-FOXA2 (1/200; Abcam); goat anti-Brachyury (T; 1/500; R&D Systems); rabbit anti–N-Cadherin (1/100) and rabbit anti-RAB11 (1/200; Cell Signaling); rabbit anti–phospho-histone H3 (1/500; Millipore); from Sigma-Aldrich, rabbit anti-LAMININ (1/500) and mouse anti-VINCULIN (1/200); from Thermo Fisher Scientific, rabbit-anti-GFP (1/1,000; Life Technologies) and mouse anti-ZO-1 (1/200; Zymed); from BD Biosciences, goat anti-SOX17 (1/200), mouse anti-E-Cadherin (1/400), mouse anti-GM130 (1/1,000), and mouse anti-PAXILLIN (1/200). Rhodamine-conjugated phalloidin (1/1,000) and secondary antibodies (1/1,000; Alexa Fluor 488, 568, 594, 633, or 647) were obtained from Thermo Fisher Scientific. HRP-conjugated secondary antibodies for Western blots were from GE Healthcare and used at 1/10,000.

SEM. Embryos for SEM were dissected in 1× PBS at room temperature and directly fixed in half-strength Karnovsky's fixative (2% PFA, 2.5% glutaraldehyde, and 0.1 M cacodylate buffer) (EIectron Microscopy Sciences) overnight or longer at 4 °C and processed as previously described (57). SEM embryos were observed using Zeiss SUPRA 25 FESEM.

Protein Alignment and Statistical Analysis. Multiple protein alignment was performed using the Clustal Omega tool (EMBL) and the BoxShade server. Two groups of data were compared using a two-tailed Student's *t* test with a cutoff for significance of <0.05 (Excel or Prism software; GraphPad). The data are presented as the mean $\pm$ SD.

ACKNOWLEDGMENTS. We thank the Mouse Genetics, Molecular Cytology, and Integrated Genomics core facilities at MSKCC and the imaging facility at the CECAD. We thank Elizabeth Lacy (MSKCC) for the Actin-FLP mice and Antonio García de Herreros (Institut Hospital del Mar d'Investigacions Mèdiques) for the SNAIL1 antibody. This work was supported by NIH Grant R37 HD03455 (to K.V.A.), MSKCC Cancer Center Support Grant P30 CA008748, and a grant from the MSKCC Center for Metastasis Research (to K.V.A.). H.B. was supported by National Kidney Foundation and National Research Service Award postdoctoral fellowships, as well as by startup funding from the medical faculty of the University Hospital of Cologne. The funders had no role in study design, data collection and analysis, decision to publish, or preparation of the manuscript.

1. Rivera-Pérez JA, Hadjantonakis AK (2014) The dynamics of morphogenesis in the early mouse embryo. *Cold Spring Harb Perspect Biol* 7:a015867.
2. Ramkumar N, Anderson KV (2011) SnapShot: Mouse primitive streak. *Cell* 146: 488–488.e2.
3. Viotti M, Nowotschin S, Hadjantonakis AK (2014) SOX17 links gut endoderm morphogenesis and germ layer segregation. *Nat Cell Biol* 16:1146–1156.
4. Ramkumar N, et al. (2016) Crumbs2 promotes cell ingression during the epithelial-to-mesenchymal transition at gastrulation. *Nat Cell Biol* 18:1281–1291.
5. Kinder SJ, et al. (1999) The orderly allocation of mesodermal cells to the extraembryonic structures and the anteroposterior axis during gastrulation of the mouse embryo. *Development* 126:4691–4701.
6. Yamanaka Y, Tamplin OJ, Beckers A, Gossler A, Rossant J (2007) Live imaging and genetic analysis of mouse notochord formation reveals regional morphogenetic mechanisms. *Dev Cell* 13:884–896.
7. Balmer S, Nowotschin S, Hadjantonakis AK (2016) Notochord morphogenesis in mice: Current understanding and open questions. *Dev Dyn* 245:547–557.
8. Lee JD, Silva-Gagliardi NF, Tepass U, McGlade CJ, Anderson KV (2007) The FERM protein Epb4.1l5 is required for organization of the neural plate and for the epithelial-mesenchymal transition at the primitive streak of the mouse embryo. *Development* 134: 2007–2016.
9. Ciruna B, Rossant J (2001) FGF signaling regulates mesoderm cell fate specification and morphogenetic movement at the primitive streak. *Dev Cell* 1:37–49.
10. Burdsal CA, Damsky CH, Pedersen RA (1993) The role of E-cadherin and integrins in mesoderm differentiation and migration at the mammalian primitive streak. *Development* 118:829–844.
11. Chuai M, Weijer CJ (2009) Regulation of cell migration during chick gastrulation. *Curr Opin Genet Dev* 19:343–349.
12. Migeotte I, Grego-Bessa J, Anderson KV (2011) Rac1 mediates morphogenetic responses to intercellular signals in the gastrulating mouse embryo. *Development* 138:3011–3020.
13. Rakeman AS, Anderson KV (2006) Axis specification and morphogenesis in the mouse embryo require Nap1, a regulator of WAVE-mediated actin branching. *Development* 133:3075–3083.
14. Madsen CD, et al. (2015) STRIPAK components determine mode of cancer cell migration and metastasis. *Nat Cell Biol* 17:68–80.
15. Castets F, et al. (1996) A novel calmodulin-binding protein, belonging to the WD-repeat family, is localized in dendrites of a subset of CNS neurons. *J Cell Biol* 134:1051–1062.
16. Moreno CS, et al. (2000) WD40 repeat proteins striatin and S/G_2 nuclear autoantigen are members of a novel family of calmodulin-binding proteins that associate with protein phosphatase 2A. *J Biol Chem* 275:5257–5263.
17. Goudreault M, et al. (2009) A PP2A phosphatase high density interaction network identifies a novel striatin-interacting phosphatase and kinase complex linked to the cerebral cavernous malformation 3 (CCM3) protein. *Mol Cell Proteomics* 8:157–171.
18. Hwang J, Pallas DC (2014) STRIPAK complexes: Structure, biological function, and involvement in human diseases. *Int J Biochem Cell Biol* 47:118–148.
19. Virshup DM, Shenolikar S (2009) From promiscuity to precision: Protein phosphatases get a makeover. *Mol Cell* 33:537–545.
20. Sangodkar J, et al. (2016) All roads lead to PP2A: Exploiting the therapeutic potential of this phosphatase. *FEBS J* 283:1004–1024.
21. Shi Z, Jiao S, Zhou Z (2016) STRIPAK complexes in cell signaling and cancer. *Oncogene* 35:4549–4557.
22. Gordon J, et al. (2011) Protein phosphatase 2a (PP2A) binds within the oligomerization domain of striatin and regulates the phosphorylation and activation of the mammalian Ste20-like kinase Mst3. *BMC Biochem* 12:54.
23. Xiang Q, Rasmussen C, Glass NL (2002) The ham-2 locus, encoding a putative transmembrane protein, is required for hyphal fusion in *Neurospora crassa*. *Genetics* 160:169–180.
24. Kemp HA, Sprague GF, Jr (2003) Far3 and five interacting proteins prevent premature recovery from pheromone arrest in the budding yeast *Saccharomyces cerevisiae*. *Mol Cell Biol* 23:1750–1763.
25. Fu C, et al. (2011) Identification and characterization of genes required for cell-to-cell fusion in *Neurospora crassa*. *Eukaryot Cell* 10:1100–1109.
26. Pracheil T, Thornton J, Liu Z (2012) TORC2 signaling is antagonized by protein phosphatase 2A and the Far complex in *Saccharomyces cerevisiae*. *Genetics* 190: 1325–1339.
27. Pracheil T, Liu Z (2013) Tiered assembly of the yeast Far3-7-8-9-10-11 complex at the endoplasmic reticulum. *J Biol Chem* 288:16986–16997.
28. Maheshwari R, Pushpa K, Subramaniam K (2016) A role for post-transcriptional control of endoplasmic reticulum dynamics and function in *C. elegans* germline stem cell maintenance. *Development* 143:3097–3108.
29. García-García MJ, et al. (2005) Analysis of mouse embryonic patterning and morphogenesis by forward genetics. *Proc Natl Acad Sci USA* 102:5913–5919.
30. Skarnes WC, et al. (2011) A conditional knockout resource for the genome-wide study of mouse gene function. *Nature* 474:337–342.
31. Testa G, et al. (2004) A reliable lacZ expression reporter cassette for multipurpose, knockout-first alleles. *Genesis* 38:151–158.
32. Hayashi S, Lewis P, Pevny L, McMahon AP (2002) Efficient gene modulation in mouse epiblast using a Sox2Cre transgenic mouse strain. *Mech Dev* 119:S97–S101.
33. Ramkumar N, et al. (2015) Protein O-glucosyltransferase 1 (POGLUT1) promotes mouse gastrulation through modification of the apical polarity protein CRUMBS2. *PLoS Genet* 11:e1005551.
34. Acloque H, et al. (2011) Reciprocal repression between Sox3 and snail transcription factors defines embryonic territories at gastrulation. *Dev Cell* 21:546–558.
35. Kwon GS, Viotti M, Hadjantonakis AK (2008) The endoderm of the mouse embryo arises by dynamic widespread intercalation of embryonic and extraembryonic lineages. *Dev Cell* 15:509–520.
36. Bai SW, et al. (2011) Identification and characterization of a set of conserved and new regulators of cytoskeletal organization, cell morphology and migration. *BMC Biol* 9:54.
37. Keller R, et al. (2000) Mechanisms of convergence and extension by cell intercalation. *Philos Trans R Soc Lond B Biol Sci* 355:897–922.
38. Yen WW, et al. (2009) PTK7 is essential for polarized cell motility and convergent extension during mouse gastrulation. *Development* 136:2039–2048.
39. Eden M, et al.; German Mouse Clinic Consortium (2016) Myoscape controls cardiac calcium cycling and contractility via regulation of L-type calcium channel surface expression. *Nat Commun* 7:11317.
40. Wagh V, et al. (2014) Fam40b is required for lineage commitment of murine embryonic stem cells. *Cell Death Dis* 5:e1320.
41. Dickinson ME, et al.; International Mouse Phenotyping Consortium; Jackson Laboratory; Infrastructure Nationale PHENOMIN, Institut Clinique de la Souris (ICS); Charles River Laboratories; MRC Harwell; Toronto Centre for Phenogenomics; Wellcome Trust Sanger Institute; RIKEN BioResource Center (2016) High-throughput discovery of novel developmental phenotypes. *Nature* 537:508–514.
42. Götz J, Probst A, Ehler E, Hemmings B, Kues W (1998) Delayed embryonic lethality in mice lacking protein phosphatase 2A catalytic subunit Calpha. *Proc Natl Acad Sci USA* 95:12370–12375.
43. Gu P, Qi X, Zhou Y, Wang Y, Gao X (2012) Generation of Ppp2Ca and Ppp2Cb conditional null alleles in mouse. *Genesis* 50:429–436.
44. Lange L, et al. (2017) Patterning and gastrulation defects caused by the t(w18) lethal are due to loss of Ppp2r1a. *Biol Open* 6:752–764.
45. Dunn LC, Bennett D (1960) A comparison of the effects, in compounds, of seven genetically similar lethal T alleles from populations of wild house mice. *Genetics* 45:1531–1538.
46. Sugimoto M (2014) Developmental genetics of the mouse t-complex. *Genes Genet Syst* 89:109–120.
47. Moser GC, Gluecksohn-Waelsch S (1967) Developmental genetics of a recessive allele at the complex T-locus in the mouse. *Dev Biol* 16:564–576.
48. Spiegelman M, Bennett D (1974) Fine structural study of cell migration in the early mesoderm of normal and mutant mouse embryos (T-locus: t-9/t-9). *J Embryol Exp Morphol* 32:723–728.
49. Hyodo T, et al. (2012) Misshapen-like kinase 1 (MINK1) is a novel component of striatin-interacting phosphatase and kinase (STRIPAK) and is required for the completion of cytokinesis. *J Biol Chem* 287:25019–25029.
50. Xue Y, et al. (2001) Mesodermal patterning defect in mice lacking the Ste20 NCK interacting kinase (NIK). *Development* 128:1559–1572.
51. Vitorino P, et al. (2015) MAP4K4 regulates integrin-FERM binding to control endothelial cell motility. *Nature* 519:425–430.
52. Yue J, et al. (2014) Microtubules regulate focal adhesion dynamics through MAP4K4. *Dev Cell* 31:572–585.
53. Sakai K, Miyazaki Ji (1997) A transgenic mouse line that retains Cre recombinase activity in mature oocytes irrespective of the cre transgene transmission. *Biochem Biophys Res Commun* 237:318–324.
54. Rodríguez CI, et al. (2000) High-efficiency deleter mice show that FLPe is an alternative to Cre-loxP. *Nat Genet* 25:139–140.
55. Eggenschwiler JT, Anderson KV (2000) Dorsal and lateral fates in the mouse neural tube require the cell-autonomous activity of the open brain gene. *Dev Biol* 227: 648–660.
56. Horzum U, Ozdil B, Pesen-Okvur D (2014) Step-by-step quantitative analysis of focal adhesions. *MethodsX* 1:56–59.
57. Huangfu D, et al. (2003) Hedgehog signalling in the mouse requires intraflagellar transport proteins. *Nature* 426:83–87.